Energy Conversion and Management 86 (2014) 944–951

Contents lists available at ScienceDirect

Energy Conversion and Management

journal homepage: www.elsevier.com/locate/enconman

Effects of environmental factors on the conversion efficiency of solar thermoelectric co-generators comprising parabola trough collectors and thermoelectric modules without evacuated tubular collector

Chao Li [a,b], Ming Zhang [c], Lei Miao [a,*], Jianhua Zhou [a], Yi Pu Kang [d], C.A.J. Fisher [e], Kaoru Ohno [c], Yang Shen [f], Hong Lin [f]

[a] Key Laboratory for Renewable Energy, Guangzhou Institute of Energy Conversion, Chinese Academy of Sciences, No. 2 Nengyuan Road, Tianhe District, Guangzhou 510640, PR China
[b] Graduate University of Chinese Academy of Sciences, Beijing 100049, PR China
[c] Department of Physics, Graduate School of Engineering, Yokohama National University, Yokohama 240-8501, Japan
[d] Department of Frontier materials, Graduate School of Engineering, Nagoya Institute of Technology, Gokiso-cho, Showa-ku, Nagoya 466-8555, Japan
[e] Japan Fine Ceramics Center, 2-4-1 Mutsuno, Atsuta-ku, Nagoya 456-8587, Japan
[f] State Key Laboratory of New Ceramic and Fine Processing, Tsinghua University, Beijing 100084, PR China

ARTICLE INFO

Article history:
Received 24 January 2014
Accepted 2 June 2014
Available online 9 July 2014

Keywords:
Solar thermoelectric conversion
Parabolic trough concentrator
Environmental factors
Solar insolation
Thermal power generation
Co-generator system

ABSTRACT

Solar thermoelectric co-generators (STECGs) are an attractive means of supplying electric power and heat simultaneously and economically. Here we examine the effects of environmental factors on the conversion efficiencies of a new type of STECG comprising parabolic trough concentrators and thermoelectric modules (TEMs). Each TEM array was bonded with a solar selective absorber plate and directly positioned on the focal axis of the parabolic concentrator. Glass tubular collectors were not used to encase the TEMs. Although this makes the overall system simpler, the environmental effects become significant. Simulations show that the performance of such a system strongly depends on ambient conditions such as solar insolation, atmospheric temperature and wind velocity. As each of these factors increases, the thermal losses of the STECG system also increase, resulting in reduced solar conversion efficiency, despite the increased radiation absorption. However, the impact of these factors is relatively complicated. Although the electrical efficiency of the system increases with increasing solar insolation, it decreases with increasing ambient temperature and wind velocity. These results serve as a useful guide to the selection and installation of STECGs, particularly in Guangzhou or similar climate region.

1. Introduction

Solar thermoelectric co-generators (STECGs) are an attractive technology for both electric and thermal power generation because they reduce relying on fossil fuels, particularly in developing economies, and have low manufacturing and installation costs. Recent attention on solar power technology reflects the many advantages of utilizing a renewable and sustainable energy sources, namely sunlight. As the vastest and most widely distributed source of energy accessible from Earth, a large number of technology can be exploited to utilize solar energy, for example, solar water heating system [1,2], A variety of photovoltaic (PV) technology [3,4], solar thermal power generation (STPG) [5,6], solar drying system [7,8], and a wide array of passive and active solar architectures [9,10], making its utilization a high priority for developing and advanced economies alike.

In order to achieve sufficiently large temperature differentials to facilitate thermoelectric conversion, solar radiation must be concentrated. Among all the solar power concentrating technologies available, parabolic trough technology has been the longest on the market [2,11–15]. In contrast to other technologies, such as solar towers, dish-Stirling systems, and Fresnel lens systems, parabolic trough technology is already developed for large-scale commercial base use, and thus represents one of the most mature technologies for concentrating solar irradiation. This technology makes essentially use of parabolic mirrors, lined up in rows, to concentrate solar irradiation up to 80 times at the absorber receiver; in theory it is possible to obtain a concentration ratio greater than 100 [2,14]. Parabolic trough collectors only having a single axis, are equipped with a solar sun tracking system to ensure that the

* Corresponding author. Tel./fax: +86 20 87035351.
E-mail address: miaolei@ms.giec.ac.cn (L. Miao).

http://dx.doi.org/10.1016/j.enconman.2014.06.010
0196-8904/

Nomenclature

Q_{solar}	total solar thermal energy
Q_{therm}	utilizing solar thermal energy
Q_{loss}	energy loss
Q_u	energy utilized cold tank
I	solar radiation intensity
A_{trough}	open area of the collecting mirror
A_p	area of the SSA
A_{Al}	area of Al plate side
d	width of the SSA
L	length of the SSA
d_{Al}	Al plate side thin
C	concentration ratio
f_{ref}	reflection factor of the PTC
α_T	solar absorbance of the SSA
σ	Stefan–Boltzmann constant
ε_E	effective emissivity
ε_T	emissivity of SSA
ε_m	emissivity of mirror
ε_{Al}	Al emissivity
h_w	convective heat exchange factor
$h_{r,Al\text{-}a}$	radiation heat exchange factor between the Al plate side and environment
$h_{r,p\text{-}tro}$	radiation heat exchange factor between the SSA and collecting mirror
v_{wind}	wind velocity
T_H	temperature of TEM's hot side,
T_C	temperature of TEM's cold side
T_p	temperature of SSA
T_{tro}	temperature of collecting mirror
T_{Al}	Al alloy plate side temperature
T_a	environmental temperature
R	total thermal resistance
R_{Al}	thermal resistance of an Al plate
R_{TE}	thermal resistance of the TEM
R_f	thermal resistance of the cold tank
R_e	internal resistance of TEM
K	thermal conductivity
I_c	current
η_{solar}	efficiency of utilizing solar thermal energy
η_{TE}	conversion efficiency of TEM
η_{ele}	electrical efficiency of the STECG

sunlight is continuously and mostly absorbed on the linear receiver installed along the focal axis of the parabolic trough mirror.

Generating electricity of thermoelectric (TE) module is based on a thermal gradient of two elements comprising different materials respectively (metal alloy or semiconductor), in which heat energy immediately converts into electricity by the difference of charge carriers velocity, namely the Seebeck effect [16]. It thus has a number of advantages over PV and STPG technology in terms of solar energy utilization, including its simple structure, lack of moving parts, silent operation, and good thermal stability. Environmentally harmless materials with high Seebeck coefficients are also being actively developed toward to lower costs devices.

The first solar thermoelectric co-generator (STECG) was constructed in 1954 by Telkes [17] comprising a flat-plate glazed collector and a thermoelectric module. Since then, this type of system has been developed on-and-off for over half a century. The significant improvements in the figure-of-merit of recently developed thermoelectric materials with low-dimensional structures, particularly those incorporating novel nanostructure [18–21], has helped to reignite interest in STECGs. Although most thermoelectric modules (TEMs) are used in waste heat recovery and hybrid devices [22,23], Kraemer's demonstration of a flat-panel STECG utilizing high-performance nanostructured TE materials with the highest efficiency of 4.6% under 1000 W/m^{-2} of solar insolation [24] represents a significant advance in STECG technology.

Parabolic trough concentrators (PTC) provide a possible way for scaling up production of STECGs. In an earlier study we confirmed the feasibility of using a STECG system consisting of TEMs in sealed glass tubular collectors which is fixed on a focal axis of PTC [25]. From the point of view of cost, ease-of-operation and system simplicity, our pilot set-up, with the rectangular aperture oriented in an east–west direction with one-axis tracking, was found to be highly practical with good performance. The TEM arrays were bonded to the solar selective absorber plate set directly on the focal axis of the parabolic concentrator. To lower the costs further, in this study we removed the evacuated tube, resulting in placing the selective absorber plate (SSA), and TEMs sandwiched by SSA and heat sink to keep direct contact with the surrounding environment. Although the overall system is much simpler, environmental factors were found to affect the efficiencies and outputs significantly. Here we present a simulation model for predicting the efficiency of STECGs under environmental conditions typically encountered in subtropical climates, specifically solar insolation, temperature and wind velocity ranges, involving heat transfer theory and energy conversation equations [26,27]. The calculation method used is suitable not only for PTC-type STECGs but for other types of STECGs also.

The set-up for our latest system is described in Section 2, along with the components of the model used to simulate environmental effects. Results from numerical simulations and thermodynamic analysis are presented in Section 3. It is found that solar efficiency is strongly dependent on wind velocity, while electrical efficiency is strongly dependent on solar insolation. In other words, solar insolation and wind velocity play an important role in the system efficiency of STECG systems. Our model provides a useful means for assessing suitable sites for installing STECGs to obtain optimal performance and thereby stimulate further development and increased production to promote rapid commercialization of these types of solar thermal generators.

2. Structure and basic thermodynamics theory of system

Fig. 1 shows the pilot set-up, which comprises 10 TEMs array with a parabolic trough concentrator but without evacuated tubular collectors. The representative parameters of the STECG and TEMs are listed in Table 1 [28,29]. TEMs are sandwiched in solar selective absorber (SSA) plate (Al alloy plate coated with SSA) and cold tank, for power generation. The hot conjunction of TEMs is attached tightly to the reverse side of SSA fin, which faces to the PTC. The hot conjunction of TEMs is attached tightly to the reverse side of SSA fin, which faces to the PTC. While the cold conjunction of TEM is bonded tightly to the cold tank oriented directly to the sky. And sandwich structure is directly positioned on the focal axis of the PTC. The SSA is heated by focused solar energy, transmitting heat to the TEM through the Al alloy fin of SSA, and the cold water tank chills the cold conjunction of TE. Consequently temperature difference between the two sides of the TEMs is assured and it generates thermo-electrical motive force through TEMs. Meanwhile,

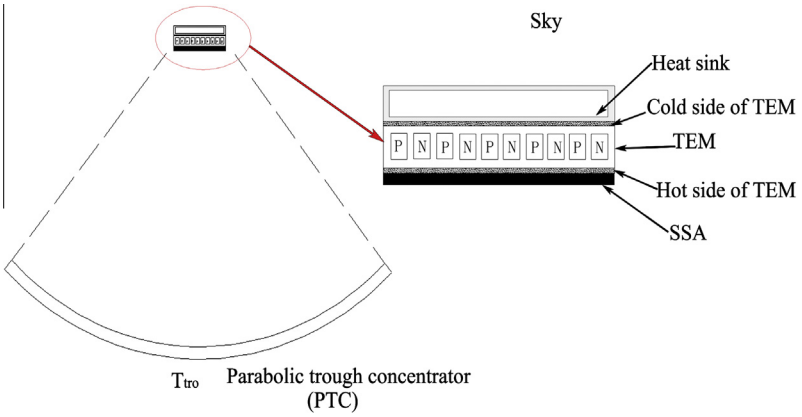

Fig. 1. Schematic diagram of a prototype cogeneration STECG, consisting of a sandwiched structure of SSA, TEMs and heat sink fixed along the focal axis of the PTC. The right-hand side shows a magnified view of the cross sectional view of the solar collector with sandwiched structure, in which a TEM is directly bonded onto the SSA.

Table 1
Geometrical and physical parameters of the STECG system.

α_T [28]	ε_T [28]	ε_{Ag} [29]	ε_{Al} [29]	L (m)	D (m)	d_{Al} (m)	f_{ref} [29]	Number of TEMs	ZT_M
0.94	0.05	0.02	0.07	2	0.06	0.025	0.92	10	0.64

the water in the tank is heated, even if TEM's thermal-to-electrical conversion is lower than 10%. The produced hot water can be used to store the residual energy. However, the removing of the evacuated tube from the system means the TEM arrays are exposed directly to the environment. This greatly alters the efficiency of the power generation system depending on changes of environmental factors, such as solar insolation, wind velocity, ambient temperature and other weather conditions (precipitation and etc.). To analyze the thermal loss and efficiency of this prototype STECG, we developed a model to simulate the effects of different weather conditions by considering the overall energy balance and heat transfer. The single-node temperature model (Fig. 2(a)) and equivalent thermal network (Fig. 2(b)) used for this purpose. And those are schematically shown in Fig. 2. This diagram shows that the solar energy (Q_{solar}) is absorbed on the SSA, meanwhile, converted into thermal energy (Q_{therm}). The collected solar thermal energy by SSA is divided in two thermal circuit: one part of the energy is utilized to generate power (Q_{TE}) by TEMs and finally heat the circulating water in the cold tank (Q_u); other part is finally dispersed to the atmosphere, namely the waste heat (Q_{loss}), through radiation heat transfer between SSA and PTC, and wind heat transfer between SSA and environment.

To estimate the effects of environmental factors on the conversion efficiency of the newly designed STECG, the following assumptions were made [25,30]:

(1) The system instantaneously reaches steady state during the heat transfer process;
(2) Thermal and radiation properties of the system elements do not depend on temperature;
(3) The parameters of the TEM are uncorrelated, which include Seebeck coefficient, electrical conductivity and thermal conductivity of thermocouple materials;
(4) Temperature difference in Al plates along the axis of PTC is negligibly small, thus conduction heat transfer is not considered;
(5) For large concentration ratio of used PTC, the aperture diameter is far beyond the thickness and width of the SAS/Al alloy plate.

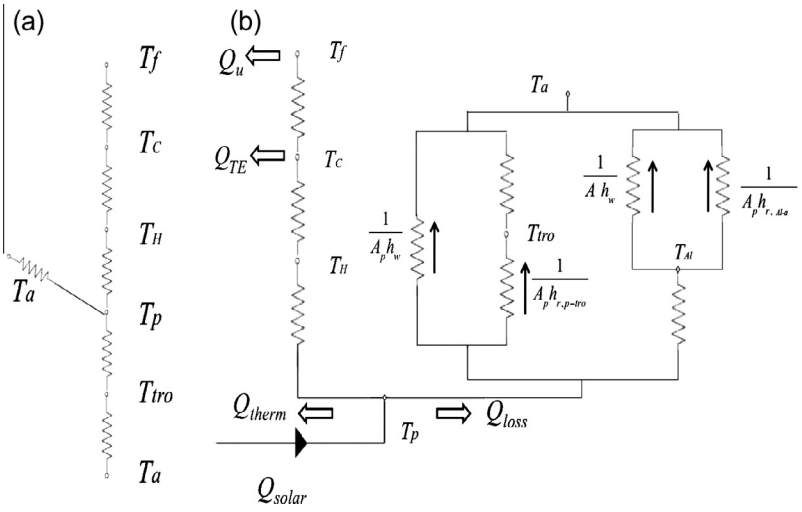

Fig. 2. (a) Single-temperature-node model used in system thermal analysis; and (b) the overall equivalent thermal network of the system.

2.1. Solar energy absorbed on the SSA

The total solar thermal energy (Q_{solar}) gathered at the SSA is expressed as

$$Q_{solar} = I\,A_{trough} f_{ref}\,\alpha_T = I\,f_{ref} A_p \alpha_T C = I\,f_{ref}\alpha_T (d \times L) C \quad (1)$$

where I is solar radiation intensity; A_{trough} is the aperture cross-sectional area of the PTC mirror; f_{ref} is the reflection factor of the PTC; α_T is the solar absorbance of the SSA; A_p is the area of the SSA; C is the concentration ratio of the STECG system defined by A_p/A_{trough}; d is the width of the SSA; and L is the length of the SSA.

2.2. Thermal losses

Through radiation heat transfer and convective heat transfer, the solar energy collected is partially dispersed into the atmosphere. Based on the temperature node model illustrated in Fig. 2, we used a simple correction to the approximate equation described in solar engineering book [31] to obtain the heat transfer coefficient of the system as follows [26,27]:

(1) The radiation heat exchange factor between the SSA and collecting mirror, through the temperature of SSA (T_p) and the temperature of collecting mirror (T_{tro}), is expressed as [31]

$$h_{r,p-tro} = \sigma \varepsilon_E (T_p^2 + T_{tro}^2)(T_p + T_{tro}) \quad (2)$$

where σ represents radiation constant, namely, the Stefan–Boltzmann constant ($5.67 \times 10^{-8}\,W/m^2\,K^4$), ε_E is effective emissivity, given by

$$1/\varepsilon_E = (1/\varepsilon_T) + (1/\varepsilon_m) - 1 \quad (3)$$

where ε_T is emissivity of SSA, and ε_m is emissivity of PTC mirror.

(2) The radiation heat exchange factor between the Al alloy plate side and environment ($h_{r,Al\text{-}a}$), can be given through Al alloy plate temperature (T_{Al}) and environment temperature (T_a)

$$h_{r,Al-a} = \sigma \varepsilon_{Al} (T_{Al}^2 + T_a^2)(T_{Al} + T_a) \quad (4)$$

where ε_{Al} is Al emissivity. Al plate side is relatively thin (d_{Al}). Thus the temperature of Al plate side with equal length of L and area of $A_{Al} = d_{Al} * L$, can be equal to T_p.

(3) The convective heat exchange factors between the SSA and surroundings, and between Al plate side and environment are represented by the empirical formula [31]

$$h_w = 5.7 + 3.8\,v_{wind} \quad (5)$$

where v_{wind} is the wind velocity in m/s.

(4) Some portion of thermal loss, such as radiation heat exchange between the sink and sky, and radiation heat exchange between lateral faces of the module and the surroundings, are negligible compared with the above heat transfer losses. When the system is in steady state, the temperature of the PTC mirror should be constant and is approximately equal to the ambient temperature, T_a.

Thus the energy loss Q_{loss} can be expressed as

$$Q_{loss} \approx h_{r,p-tro} A_p (T_p - T_{tro}) + h_w A_p (T_p - T_a) + 2h_{r,Al-a} A_{Al} (T_{Al} - T_a) + 2h_w A_{Al} (T_{Al} - T_a) \quad (6)$$

The energy conservation equation of the system thus becomes

$$Q_{solar} = Q_{loss} + Q_{therm} \quad (7)$$

2.3. Thermal resistances

In the STECG system, the temperature difference between the SSA plate and the tank results in thermal diffusion. The thermal power Q_{therm} is thus given by

$$Q_{therm} = (T_p - T_a)/R \quad (8)$$

Here R is the thermal resistance between the SSA of the Al plates and water. Q_{therm} is consumed for both TEM conversion and heating of the cooling water in the tank. Q_{therm} is a significant energy to evaluate the system performance of a STECG.

The main resistances which affect the efficiency of the system are R_{Al}, the thermal resistance of an Al plate bonded on the SSA; R_{TE}, the thermal resistance of the TEM component; and R_f, the thermal resistance of the cold tank. R can thus be rewritten by

$$R = R_{Al} + R_{TE} + R_f \quad (9)$$

The calculated thermal resistance values used in this study are summarized in Table 2 (Support information).

2.4. Solar conversion efficiency

As mentioned earlier, the collected solar thermal energy at the SSA (Q_{therm}) is utilized to generate electricity in TEM and to heat water simultaneously. The efficiency of utilizing solar thermal energy in this way is given by

$$\eta_{solar} = Q_{therm}/IdLC \quad (10)$$

where the thermal power Q_{therm} utilized by the system is given approximately by Eqs. (6) and (7).

2.5. Electrical conversion efficiency

The thermal energy of electricity generated by the TEM, Q_{TE}, can be obtained from the Peltier effect, heat transfer process and the Joule effect [16] according to

$$Q_{TE} = SI_C T_H + K(T_H - T_C) - \frac{1}{2} I_C^2 R_e \quad (11)$$

The heat transfer components in a TEM are complex and interrelated, especially the Peltier heat, Seebeck heat and Joule heat. Thus Q_{TE} is difficult to calculate from Eq. (11). However, Q_{therm} is not dissipated through Al alloy plate, so Q_{TE} can be equal to the solar energy collected by the SSA, i.e., $Q_{TE} = Q_{therm}$.

According to the text book on thermo electricity [16], the TEM's thermoelectric conversion efficiency is given by

$$\eta_{TE} = (T_H - T_C)\left(\sqrt{1 + ZT_M} - 1\right)/T_H\left(\sqrt{1 + ZT_M} + T_H/T_C\right) \quad (12)$$

where $T_M = (T_H + T_C)/2$. In Eq. (14), the Joule heat generated in the TEM is already taken into account.

T_H and T_C are easily obtained from equations describing heat conduction in the system by:

$$T_H = T_p - R_{Al} Q_{therm} \quad \text{or} \quad T_H = T_a + (R_f + R_{TE}) Q_{therm} \quad (13)$$

$$T_C = T_p - (R_{Al} + R_{TE}) Q_{therm} \quad \text{or} \quad T_C = T_a + R_f Q_{therm} \quad (14)$$

The electrical efficiency of the STECG can be expressed as the percentage of the generated electrical energy and the total incidence of solar energy on PTC,

$$\eta_{ele} = Q_{TE}\eta_{TE}/IdLC \quad (15)$$

3. Simulation results and discussion

Based on the equations related to solar heat conduction and thermodynamic equilibrium theory discussed above, the effects

Table 2
Thermal resistance values (K/W) used in modeling the STECG system.

R_{Al}	R_{TE}	R_f
0.002	0.65	0.02

of environmental factors such as solar intensity, environmental temperature, and wind velocity on the efficiency of STECGs without evacuated tube and the associated thermal losses of the prototype system were investigated. Because solar thermal energy is a form of "low-grade (high entropy)" energy, a larger concentration ratio is commonly used to enhance the collected energy for higher temperature usage. A comprehensive examination of the TEM performance and applicable temperatures is required before determining whether such technology is necessary or not.

Fig. 3 shows the electrical efficiency and the SSA temperature at different concentration ratios for the TEMs with ZT = 0.64, a solar insolation of 1000 W/m^2, wind velocity of 2.5 m/s, and ambient temperature of 296 K. When the concentration ratio is larger than 100, the temperature of the SSA exceeds 1000 K, suggesting very good performance can be achieved. High-temperature thermoelectric materials such as SiGe and compound oxide which is considered as suitable for the use above 1000 K, can be chosen [32,33].

To determine the optimum TEM performance, the concentration ratio value was set at 100 as a favorable value for the present simulation with single axis tracking system. For a static concentrator with no tracking, however, the maximum concentration ratio is used to be limited about 10. When single-axis tracking is introduced, a concentration ratio of 100 can be achieved, but for values greater than this dual-axis tracking systems are required [34].

The influence of environmental factors on system operation conditions were examined by simulating thermal loss trends, electrical efficiency and solar efficiency using three environmental parameters, namely solar insolation, ambient temperature and wind velocity. Weather data for Guangzhou (112°E and 22°N) was used as input to the simulation program. Details of this data are provided as Supporting information. According to the weather data, the simulation results can be adapted to use in Guangzhou or similar climate area. For each simulation, only one environmental parameter was varied while the others were held constant. Numerical analysis was performed using the thermodynamic model above discussed constructed by combining the energy conversion equation and heat transfer theory.

3.1. Effects of solar insolation

The effect of solar insolation on the thermal loss, electrical efficiency and solar efficiency are shown in Figs. 4 and 5. Solar insolation was varied from 0 to 1200 W/m^2, while temperature and wind velocity were kept constant as T_a = 293 K and v_{wind} = 2.5 m/s.

Fig. 4(a) shows that the SSA temperature (T_p) increases linearly with increasing solar insolation within the designated range. The thermal loss increases quickly with increasing of solar insolation because it varies as a function of the fourth power of T_p, as seen in Fig. 4(b). As the solar insolation is less than 600 W/m^2, the increment of the thermal losses is very slow with increasing solar insolation, but after solar insolation reaches a value around 600 W/m^2, the thermal losses increase rapidly. The solar-to-thermal conversion efficiency decreases from 66.66% to 63.28% with an increase in solar insolation as a result of thermal losses increasing from 19.82% to 23.23%.

A temperature difference across two sides of the TEM enables the system to generate electricity. It can be seen from Fig. 5 that both T_H and T_C increase when solar insolation sufficiently increase. However, the augment of T_H is greater than that of T_C, thus the temperature difference between T_H and T_C also increases and this results in a significant increase in electrical efficiency, from 1.25% to 5.68%, as seen in Fig. 5. Our model thus indicates that as solar

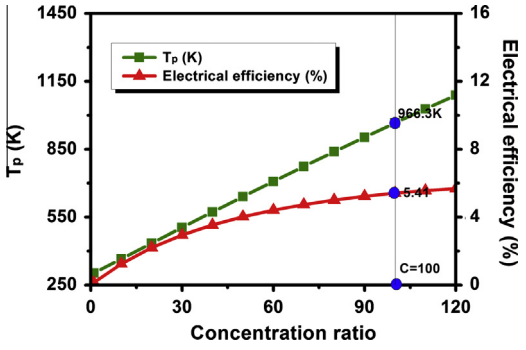

Fig. 3. Electrical efficiency and temperature of the SSA (T_p) for different concentration ratios, when the TEMs of ZT = 0.64, a solar insolation of 1000 W/m^2, wind velocity of 2.5 m/s, and ambient temperature of 296 K.

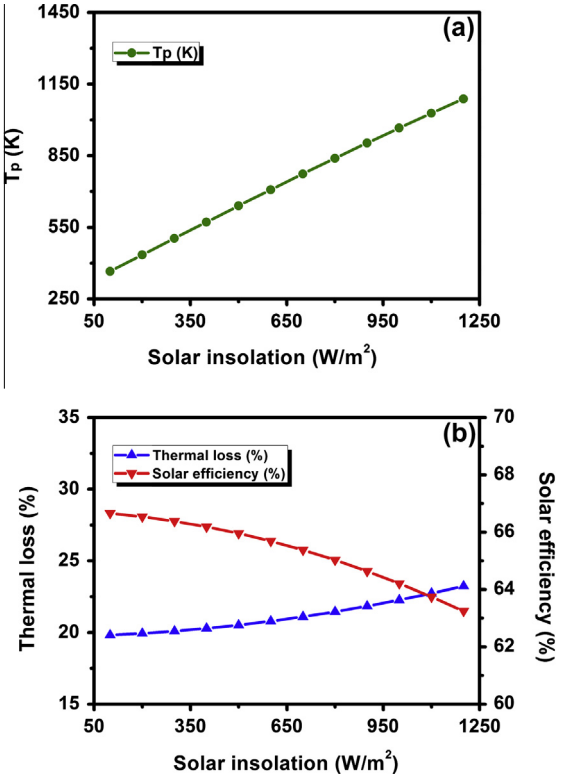

Fig. 4. (a) The temperature of the SSA (T_p) and (b) thermal loss and solar efficiency as a function of solar insolation.

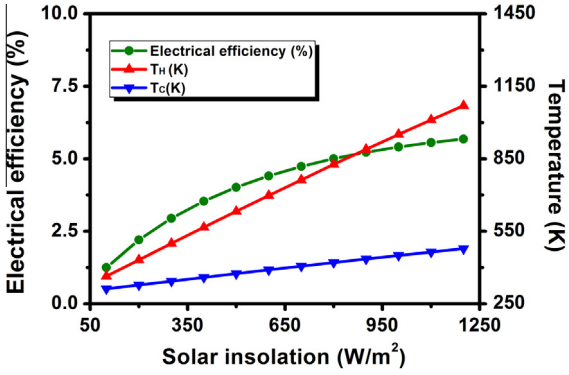

Fig. 5. The green line is the electrical efficiency vs solar insolation, and red and blue lines are the TEM's temperature of the hot and cold side vs solar insolation, respectively. (For interpretation of the references to color in this figure legend, the reader is referred to the web version of this article.)

insolation increases, electrical efficiency increases significantly while the solar-to-thermal efficiency decreases slightly as in Fig. 4b. The optimal concentration ratio needs to be determined to achieve a suitable balance between these two characteristics of the system to design a high performance STECG system.

The dissipated thermal energy also increase, however, the rate of augment in electrical energy production is greater than the rate of augment in dissipated thermal energy. Thus, improving electrical power output and electrical efficiency can be promoted by enlarging solar insolation intensity. In practice, STECG performance can be improved by addition of an effective waste heat auxiliary module or improvement in the concentration ratio for operation at night or under less powerful solar insolation conditions.

3.2. Effects of environmental temperature

The dependence of T_p, thermal losses, and solar efficiency of the STECG system on an ambient temperature ranging from 273 K to 313 K are shown in Fig. 6(a) and (b), while solar insolation (1000 W/m^2) and wind velocity (2.5 m/s) were constant. With increasing ambient temperature, T_a, T_p slowly increases to 963.5 K (Fig. 6(a)). As the radiation heat transfer coefficient and convective heat transfer coefficient are directly proportional to the cubes of T_p and T_a, respectively as seen in Eqs. (2) and (4), the thermal losses naturally increase with increasing temperature. Fig. 6(b) shows that thermal losses change slightly with different ambient temperatures. At T_a = 273 K, thermal losses are 21.48%, and when T_a = 313 K, thermal losses are 21.86%. Solar efficiencies also slightly decrease with increasing ambient temperature in the range of 63.12–62.74% in response to the small increase in thermal losses. The temperature difference between T_H and T_C is almost constant with increasing ambient temperature due to the simultaneous increase of T_H and T_C, as seen in Fig. 7. Electrical efficiency thus decreases only slightly, in the range of 5.46–5.12%.

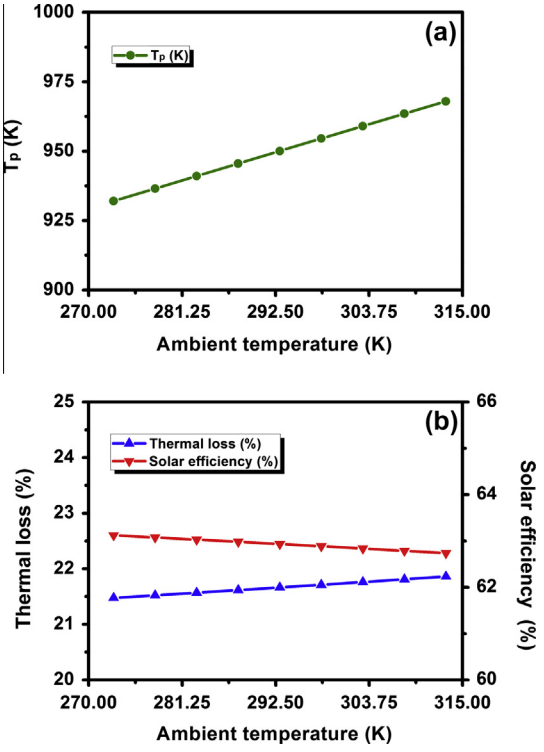

Fig. 6. (a) The temperature of the SSA (T_p) and (b) thermal losses and solar efficiency as a function of ambient temperature.

Eqs. (5) and (6) indicate that the variation of solar efficiency and electrical efficiency as a function of ambient temperature are not straightforward. However, our simulation results demonstrate that changes in ambient temperature should not have a significant effect on STECG efficiencies. The result could be caused from the small range of defined ambient temperature, and can be true.

3.3. Effects of wind velocity

Forced convection heat transfer between air and the SSA occurs when wind blows across the surfaces of the SSA. Fig. 8(a) shows the wind velocity dependence of T_p of our STECG system for different wind velocities varying from 0 to 12 m/s under solar insolation

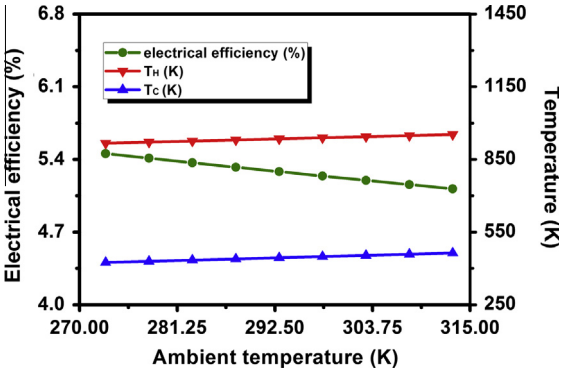

Fig. 7. The green line is the electrical efficiency vs ambient temperature, and red and blue lines are the TEM's temperature of the hot and cold side vs ambient temperature, respectively. (For interpretation of the references to color in this figure legend, the reader is referred to the web version of this article.)

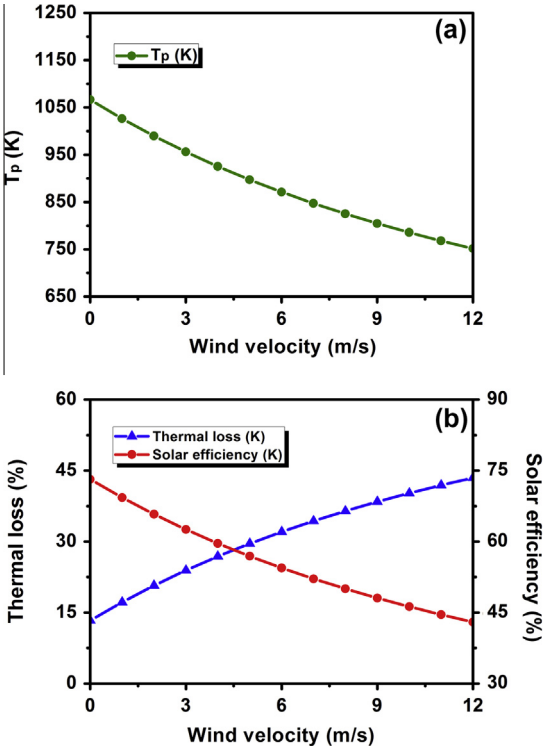

Fig. 8. (a) Thermal losses and temperature of the SSA, T_p, as a function of wind velocity. (b) The green line is the electrical efficiency vs wind velocity, and red and blue lines are the TEM's temperature of the hot and cold side vs wind velocity, respectively. (For interpretation of the references to color in this figure legend, the reader is referred to the web version of this article.)

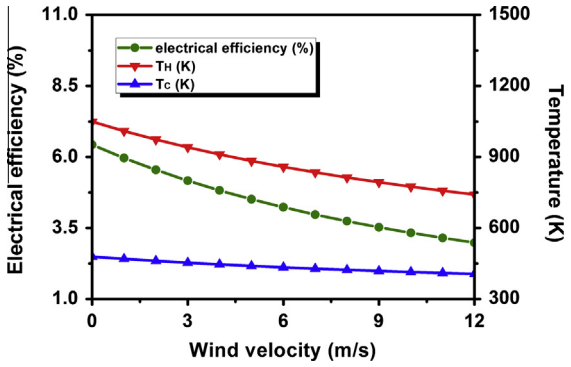

Fig. 9. The green line is the electrical efficiency vs wind velocity, and red and blue lines are the TEM's temperature of the hot and cold side vs wind velocity, respectively. (For interpretation of the references to color in this figure legend, the reader is referred to the web version of this article.)

of 1000 W/m^2 and ambient temperature at 296 K. As expected, the temperature of the SSA decreases with increasing wind velocity; for example, when the wind velocity is 12 m/s, T_p decreases to 751.75 K. This is because forced convection heat transfer increases with increasing wind velocity, and as a consequence T_p decreases mainly. An increasing convection heat transfer coefficient and radiation heat transfer should result in increasing thermal losses, leading to the reduction of the solar energy efficiency values presented in Fig. 8(b). For example, when the wind velocity is 12 m/s, the thermal loss and solar efficiency are significant at 43.49% and 42.98%, respectively.

The temperature difference across two sides (hot and cold) of the TEM and T_H rapidly decrease with increasing wind velocity as shown in Fig. 9. Due to the interdependence of electrical efficiency and temperature of the TEM, electrical efficiency decreases from 6.43% to 2.98% with an increase in the wind velocity from 0 to 12 m/s.

Wind velocity thus has a large impact on solar-to-thermal conversion efficiency and consequently effect on electrical efficiency for fixed values of solar insolation and environmental temperature. For the small system, it can be concluded that the addition of evacuated tubular solar collectors to the system, as reported in detail by Miao et al. [25], is beneficial for improving the overall system efficiency of STECGs. However, it will be difficult for a long axial PTC system to add evacuated tube, because it is hard to find appropriate materials to brace sandwich structures with enough high strength to avoid deflection along longitudinal axis. Coating of the high temperature durable thermal insulation material could be a method to decrease the temperature of Al plate side.

4. Conclusions

The results of simulations of a solar co-thermoelectric generator (STECG) have been presented, constructed using a PTC and TEMs without evacuated tube. Electricity and heat can be supplied simultaneously, and the system is thus attractive as an environmentally clean and efficient co-generation system at low cost. The results show that the performance of the system strongly depends on environmental conditions. The thermal losses of the system always increase with increasing solar insolation, ambient temperature and wind velocity. However, their impact on electrical and thermal conversion efficiency is more complex. The electrical efficiency of the system increases with increasing solar insolation, but decreases with increasing environmental temperature and wind velocity.

Solar efficiency is significantly depending on wind velocity, and electrical efficiency on solar insolation. These two essential environmental factors decide fatefully the system efficiency of a STECG under realistic conditions. By combining our model with careful analysis of experimental data taken from STECGs under different climates, it should be possible to select the most suitable sites and arrangement/orientation to gain the optimum performance from the system.

Acknowledgements

This work was supported by the National Natural Science Foundation of China (Grant No. 51172234) and State Key Laboratory of New Ceramic and Fine Processing, Tsinghua University.

Appendix A. Supplementary material

Supplementary data associated with this article can be found, in the online version, at http://dx.doi.org/10.1016/j.enconman.2014.06.010.

References

[1] Yuan T, Zhao CY. A review of solar collectors and thermal energy storage in solar thermal applications. Appl Energy 2013;104:538–53.
[2] Kalogirou SA. Solar thermal collectors and applications. Prog Energy Combust Sci 2004;30:231–95.
[3] Purvins A, Papaioannou IT, Debarberis L. Application of battery-based storage systems in household-demand smoothening in electricity-distribution grids. Energy Convers Manage 2013;65:272–84.
[4] Wright M. Organic-inorganic hybrid solar cells: a comparative review. Solar Energy Mater Solar Cells 2012;107:87–111.
[5] Bakos GC, Tsechelidou C. Solar aided power generation of a 300 MW lignite fired power plant combined with line-focus parabolic trough collectors field. Renew. Energy 2013;60:540–7.
[6] Concentrated solar power. <http://enerlogy.co.za/sectors/renewables-2/solar/solar-csp/>.
[7] Rahman SMA, Saidur R. An economic optimization of evaporator and air collector area in a solar assisted heat pump drying system. Energy Convers Manage 2013;76:377–84.
[8] Sreekumar A. Techno-economic analysis of a roof-integrated solar air heating system for drying fruit and vegetables. Energy Convers Manage 2010;51:2230–8.
[9] Zain-Ahmed A, Sopian K. Daylighting as a passive solar design strategy in tropical buildings: a case study of Malaysia. Energy Convers Manage 2002;43:1725–36.
[10] Haywood A, Jon Sherbeck. Thermodynamic feasibility of harvesting data center waste heat to drive an absorption chiller. Energy Convers Manage 2012;58:26–34.
[11] Behar O, Khellaf A, Mohammedi K. A review of studies on central receiver solar thermal power plants. Renew Sust Energy Rev 2013;104:538–53.
[12] Zhang HL, Baeyens J, Degrève J, Cacères G. Concentrated solar power plants: review and design methodology. Renew Sust Energy Rev 2013;22:466–81.
[13] Geyer M. EUROTROUGH-Parabolic trough collector developed for cost efficient solar power generation. In: 11th International symposium on concentrating solar power and chemical energy technologies; 2002.
[14] Valan Arasu A, Sornakumar T. Design, manufacture and testing of fiberglass reinforced parabola trough for parabolic trough solar collectors. Sol Energy 2007;81:1273–9.
[15] Fernández-García A, Zarza E, Valenzuela L. Parabolic-trough solar collectors and their applications. Renew Sust Energy Rev 2010;14:1695–721.
[16] Rowe DM. General principles and basic considerations. In: Rowe DM, editor. Thermoelectrics handbook: macro to nano. New York: CRC Taylor & Francis Group; 2006. p. 1–3.
[17] Telkes M. Solar thermoelectric generators. J Appl Phys 1954;25:756–77.
[18] Harman TC. Quantum dot superlattice thermoelectric materials and devices. Science 2002;297:2229–32.
[19] Kanishka B, He JQ, Blum ID. High-performance bulk thermoelectrics with all-scale hierarchical architectures. Nature 2012;489:414–8.
[20] Androulakis J, Hsu KF. Nanostructuring and high thermoelectric efficiency in p-type $Ag(Pb_{1-y}Sn_y)mSbTe_{2+m}$. Adv Mater 2006;18:1170–3.
[21] Martin J, Wang L. Enhanced Seebeck coefficient through energy-barrier scattering in PbTe nanocomposites. Phys Rev B 2009;79:115311.
[22] Wang N, Han L. A novel high-performance photovoltaic-thermoelectric hybrid device. Energy Environ Sci 2011;4:3676–9.
[23] Zhang XD, Chau KT. An automotive thermoelectric–photovoltaic hybrid energy system using maximum power point tracking. Energ. Convers. Manage 2011;52:641–7.
[24] Kraemer D, Poudel B, Feng H-P. High-performance flat-panel solar thermoelectric generators with high thermal concentration. Nat Mater 2011;10:532–8.
[25] Miao L, Zhang M, Tanemura S, Tanaka T. Feasibility study on the use of a solar thermoelectric cogenerator comprising a thermoelectric module and

evacuated tubular collector with parabolic trough concentrator. J Electron Mater 2012;41:1759–65.
[26] Chen J. Thermodynamic analysis of a solar-driven thermoelectric generator. J Appl Phys 1996;79:2717–21.
[27] Amatya R, Ram RJ. Solar thermoelectric generator for micropower applications. J Electron Mater 2010;39:1735–40.
[28] Zhou WX, Shen Y, Hu ET. Nano-Cr-film-based solar selective absorber with high photo-thermal conversion efficiency and good thermal stability. Opt Express 2012;20:28953–62.
[29] Incropera Frank P, Lavine Adrienne S, DeWitt David P. Fundamentals of heat and mass transfer. John Wiley & Sons; 2011.
[30] Zhang M, Miao L, Kang YP, Tanemura S, Fisher CAJ, Xu G, et al. Efficient, low-cost solar thermoelectric cogenerators comprising evacuated tubular solar collectors and thermoelectric modules. Appl Energy 2013;109:51–9.
[31] Duffie JA, Beckman WA. Solar energy thermal processes. New York (NY): Wiley; 1974. p. 120–214 [chapter 7: flatplate collectors, chapter 8: focusing collectors].
[32] Joshi G, Lee H, Lan Y. Enhanced thermoelectric figure-of-merit in nanostructured p-type silicon germanium bulk alloys. Nano Lett 2008;8:4670–4.
[33] Fergus JW. Oxide materials for high temperature thermoelectric energy conversion. J Eur Ceram Soc 2012;32:525–40.
[34] Sala G, Pachon D, Anton I. Test, rating and specification of PV concentrator components and systems: classification of PV concentrators. Madrid: Solar Energy Institute, Polytechnic University of Madrid; 2002.